SUPPLEMENTARY METHODS

Portal vein perfusions. Mice were anesthetized with 50 µL of sodium pentobarbital (65 mg/mL) administered i.p. Once fully unconscious (approximately 5 minutes following delivery), the abdomen was sprayed with 70% ethanol, and the mouse was placed on a surgical platform within a reservoir to contain run-off buffer and body fluids. A trans-verse incision was made through the skin, fascia, and muscular layers of the lower abdomen. A lateral sagittal incision was made on each side of the body, exposing the abdominal contents. A second transverse incision was made inferiorly to the right kidney and toward the dorsal aspect of the mouse to allow the perfusion buffer and body fluids to drain from the abdomen. The portal vein was then exposed by gently moving the intestines laterally toward the left body wall. A suture needle was threaded under the portal vein and tied loosely. Next, the portal vein was cannulated with a 24-gauge catheter needle, the needle was withdrawn, and tubing with buffer was reconnected to the catheter. The abdominal aorta and inferior vena cava were cut, and the catheter was firmly tied into the portal vein. The beating heart was then exposed by cutting through the diaphragm and thorax. The right atrium was cut to prevent recirculation of buffer to the liver and to terminate perfusion to the brain. All livers were perfused with our standard oxygenated buffer pre-warmed to 42°C (determined empirically to counter heat loss in tubing such that tissue delivery is maintained at physiological temperature) with a counter-current heat-exchange circuit and a recirculating water bath. The buffer delivery is maintained at a rate of 8 mL/minute using a peristaltic pump for a period of 1 hour, unless otherwise noted. During the perfusion procedure the liver temperature is monitored periodically with a Fluke infrared thermometer (Everett, WA). An adjustable incandescent lamp is used to control the local temperature (37°C±1°C) of the liver during the procedure. Perfusate effluent from the initial 30 minutes was discarded, and effluent is collected from the final 30

minutes of the procedure. In addition, 1.8 mL collections are made at 30, 40, 50, and 60 minutes from perfusion initiation. At the completion of the perfusion procedure, the liver was freeze-clamped in a bath of liquid nitrogen. The effluent and tissue was stored at -80°C until further processing. The standard perfusion media contained Krebs-Henseleit bicarbonate buffer (118 mM NaCl, 25 mM $NaHCO_3$, 4.7 mM KCl, 0.4 mM KH_2PO_4, 2.5 mM $CaCl_2$, 1.22 mM $MgSO_4$-7•H2O, pH 7.4), 3% (v/v) ^2H_2O, 1.5 mM sodium lactate, 0.15 mM sodium pyruvate, 0.25 mM glycerol, ±0.2 mM sodium [U-$^{13}C_3$] propionate, ±0.2 mM unlabeled sodium octanoate, and ±10 μU/mL human insulin (Lilly). For unlabeled ketone body replenishment perfusion, the buffer was supplemented with either 1 mM D-βOHB/0.1 mM AcAc/0.9 mM ethanol; or 0.1 mM D-βOHB/1 mM AcAc. Ethanol included in the 1 mM D-βOHB formulation reconciles ethanol inherently present in the presence of 1 mM AcAc: base hydrolysis of ethyl AcAc was performed by addition of 50% NaOH to pH 12 and incubation at 60°C for 30 min. Base hydrolyzed AcAc was adjusted to pH 8.5, and AcAc concentration was confirmed using standard biochemical assays coupled to colorimetric substrates (Wako). A subset of perfusions incorporated the use of 0.2 mM sodium [1,2,3,4-$^{13}C_4$]octanoate; for these perfusions, neither unlabeled octanoate, sodium [U-$^{13}C_3$] propionate, nor ^2H_2O was included in the perfusion buffer. Prior to perfusion, all buffers were oxygenated for 2h at 42°C with continuous bubbling of a 95% O_2, 5% CO_2 gas mixture into the buffer reservoir using a fritted gas delivery tube.

Quantification of glucose sourcing and hepatic fluxes. To determine sourcing of glucose production, ^2H NMR collections were obtained from ^2H-labeled monoacetone glucose derivatized from hepatic venous effluent glucose selectively labeled in the liver by ^2H_2O (see below for glucose derivatization method). Specifically, the selective enrichment of position #2, #5 and #$6_{(s)}$ encodes unique biochemical pathway information that allows the contributors (glycogen, glycerol,

TCA cycle) of glucose production. Integrated intensities of signals (H_2, H_5, H_{6s}) from the ^2H NMR spectrum provide the information to calculate the relative contributions to overall glucose production **(Fig. S2B)**. For $^2H\{^1H\}$ NMR measurements, dried monoacetone glucose was dissolved in 510 μL 5% deuterium depleted H_2O (in acetonitrile) and transferred to a 5 mm 528-pp Wilmad NMR tube (Vineland, NJ). During the collection, the magnet was not maintained on a field-frequency lock, as the lock channel is used to detect the ^2H signal. Conditions included collection at 48°C over 1380 Hz using a 68 μs (90°) pulse, 1.3s delay between transients and Waltz16 decoupling on the proton channel during a 1s acquisition period. Pending signal-to-noise (S/N), 4,000-40,000 transients were collected. Magnet stability was sufficient to result in deuterium line-widths of 2-3 Hz providing for excellent peak separation for quantitation by integration to establish relative ^2H enrichments at the number 2, 5 and 6(s) positions of ^2H-labeled monoacetone glucose.

To measure [U-^{13}C]propionate incorporation into glucose produced during perfusions, ^{13}C-NMR of the #2 position of monoacetone glucose derivatized from hepatic venous effluent glucose selectively labeled by [^{13}C]propionate in the liver (see below for glucose derivatization method) obtained from the liver perfusion effluent presents as an isotopomer pattern, the individual components of which provide insight into flux through the TCA cycle as well as anaplerotic/cataplerotic pathways. The dominant singlet signal from the position #2 carbon originates from the 1.1% ^{13}C that occurs naturally from any substrate utilized in glucose production while the isotopomer pattern components originate solely from the uniformly [U-^{13}C]propionate included in the perfusion buffer. For $^{13}C\{^1H\}$ NMR studies, 40 μL of d_3-acetonitrile was added to the sample used for ^2H NMR of monoacetone [$^{13}C/^2H$]glucose, and a field-frequency lock was established during data collection at 25°C. Collection conditions included a 12 μs excitation pulse,

22,320 Hz collection window with waltz16 decoupling for ^{1}H. Pending S/N, 4,000 to 40,000 transients were collected, and signal magnitudes were established by integration **(Fig. S2C)**.

^{2}H and ^{13}C NMR methods profiling $^{13}C/^{2}H$-labeled monoacetone glucose establish the biochemical pathways important in its production (1). The flux contributions to glucose production from glycogen, glycerol and phosphoenylpyruvate (PEP) are designated by V_2, V_3 and V_4 respectively:

V_1 = hepatic glucose production (HGP), determined by ^{1}H-NMR

V_2 = flux from glycogen = $V_1 * (H_2 - H_5)/H_2$

V_3 = flux from glycerol = $2 * V_1 * (H_5 - H_{6s})/H_2$

V_4 = flux from PEP = $2 * V_1 * H_{6s}/ H_2$

From the ^{13}C NMR isotopomer information of the #2 position of glucose, flux evaluations (V_5, V_6 and V_7) can be determined for flow through pyruvate kinase and malic enzyme (pyruvate recycling), phosphoenolpyruvate carboxykinase (PEPCK) mediated flow to PEP and citrate synthase (CS) mediated flow of the TCA cycle. In these expressions D12, Q, and D23 represent the two doublet and one quartet isotopomer magnitudes (areas) originating from labeled propionate incorporated into glucose production via the TCA cycle. The isotopomer patterns result from ^{13}C spin-spin scalar coupling when labeled spins are bonded to each other. These isotopomer magnitudes (areas) can be correlated to flux through the following expressions (1).

V_5 = (pyruvate cycling flux, through pyruvate kinase and malic enzyme) = $V_4 * (D12\text{-}Q)/(Q\text{-}D23)$

V_6 = (flux through PEP carboxykinase, anaplerosis) = $V_4 * (D12\text{-}D23)/(Q\text{-}D23)$

V_7 = (flux through citrate synthase, TCA cycle flux) = $V_4 * D23/(Q\text{-}D23)$

Preparation of monoacetone glucose. The preparation of $^{13}C/^{2}H$-labeled monoacetone glucose was similar to that reported previously (1). Liver perfusion effluent media (250 mL) was thawed from -80^{o}C and reduced in volume at 45^{o}C on a R-300 Büchi rotary evaporator (Flawil,

Switzerland) equipped with a IKA recirculation chiller (Breisgau, Germany) maintained at -10°C. The residual perfusion media was then lyophilized to complete dryness. A crude extraction of $^{13}C/^{2}H$-labeled glucose was carried out by stirring the freeze-dried perfusate powder, in three repeat trials, with 10 mL of 90% methanol-10% H_2O solution for 10 minutes at room temperature. After stirring, the mixture was centrifuged and the $^{13}C/^{2}H$-labeled glucose-rich supernatant was collected. This solution was further reduced in volume and effectively desalted using a SpeedVac. This was achieved by reducing the volume to roughly 0.8-1 mL, followed by centrifugation to remove precipitated salts, and final drying for at least 10 hours at 45°C under vacuum. The recovered solids were then stirred with 3 mL of dry acetone and 120 uL of dry sulfuric acid for 4-6 hours at room temperature to produce, via condensation, a yellow-orange $^{13}C/^{2}H$-labeled diacetone glucose solution. The acidic acid solution was separated from the residual solids by filtration and combined with an equivalent volume of H_2O. While stirring, the pH of the di-acetone glucose solution was increased to 2 by addition of solid sodium carbonate (Na_2CO_3) and stirred continuously for approximately 24 hours. During this time, $^{13}C/^{2}H$-labeled diacetone glucose was converted to $^{13}C/^{2}H$-labeled monoacetone glucose. The faintly yellow or colorless monoacetone glucose solution was then further adjusted to pH 7-8 with addition of solid sodium carbonate. Crude $^{13}C/^{2}H$-labeled monoacetone glucose was recovered by stripping off the solvent at 45°C degrees using a SpeedVac. Further purification of $^{13}C/^{2}H$-labeled monoacetone glucose was achieved by five extractions using boiling ethyl acetate followed by further drying under vacuum. A final purification was carried out by reverse phase chromatography using 3 mL Discovery DSC-18 packed tubes. The $^{13}C/^{2}H$-labeled monoacetone glucose, in 0.5 mL H_2O, was loaded onto the column and eluted with 7% acetonitrile-water. ^{1}H NMR was used to optimize separation conditions, but commonly, the initial 0.7 mL were discarded, and the following 2.5-3 mL were

collected. Pure white monoacetone [$^{13}C/^{2}H$]glucose was obtained via evaporating the elution volume to dryness.

Mass spectrometry methods for untargeted metabolomics. Liquid chromatography was performed on a Dionex Ultimate 3000 RSLC using a Phenomenex Luna NH_2 column (100 mm x 1 mm, 3 µm particle size) for untargeted metabolomics. Metabolomics was carried out using hydrophilic interaction liquid chromatography (HILIC) mode, with the following mobile phase compositions: A = 95% H_2O, 5% ACN, 10 mM NH_4OAc, 10 mM NH_4OH, pH 9.5; B = 95% ACN, 5% H_2O, 10 mM NH_4OAc, 10 mM NH_4OH, pH 9.5. The extracts were separated on Luna NH_2 column using binary gradient 75-0% B for 45 min, then 0% B for 12 min, and 75%B for 13 min at 50 µL/min. Sodium [1,2,3,4-$^{13}C_4$]octanoate perfused liver extract was separated using following gradient: 75-0% B for 35 min, then 0% B for 15 min, and 75%B for 15 min at 50 µL/min. Column temperature was maintained at 30°C, and injection volume was 4 µL. MS was performed on a Thermo Q Exactive Plus with a heated ESI source. The MS was operated in negative ionization mode. MS resolution was set to 70000 and the AGC target to $3x10^6$ ions with a maximum injection time of 200 ms. The mass scan for extract analysis was 68-1020 *m/z* whereas for the 0.2 mM sodium [1,2,3,4-$^{13}C_4$]octanoate perfused liver samples was 100-1500 *m/z*. Following ESI parameters were applied: auxiliary gas 10, sweep gas 1, spray voltage -3 kV, capillary temperature 275°C, S-lens RF 50, auxiliary gas temperature 150°C, and sheath gas flow 35 (arbitrary unit).

Data (.RAW files) were converted to the mzXML format using MSConvert with the vendor pick-peaking option selected, and processed using xcmsonline or X13CMS R package as described previously (2-5). Liver metabolomics data was uploaded to xcmsonline, and analyzed based on a method “HPLC / Orbitrap - HPLC with ~60 min gradient / Orbitrap” available online

with modifications. The feature detection parameters were 5 ppm, peak width interval 10-180 min, mzdiff 0.01, signal to noise threshold 6, integration method 2, prefilter peaks 3 and prefilter intensity 500. Retention time correction was carried out using obiwarp methods and 0.5 step size (in *m/z*). Alignment bw was set to 30, mzwid to 0.025, and minfrac to 0.5. Peaks with fold change greater than 2, and p value lower than 0.05 were selected, with median fold change normalization option and unpaired parametric t-test (Welch t-test). For X13CMS, the data was processed using R studio where the XCMS (v. 1.40) package was used to pick chromatographic (method = 'centWave', ppm = 2.5, peakwidth = c(20, 180)) peaks and alignment retention time (bw=10, mzwid=0.015, retention time correction method = 'obiwarp') across samples within an experiment. X^{13}CMS (v.1.4) was used on the output to extract isotopologue groups. The parameters used for X^{13}CMS are RTwindow = 10, ppm = 5, noiseCutoff = 10000, intChoice = "intb", alpha = 0.05 within getIsoLabelReport().

Mass spectrometry methods for shotgun lipidomics. Part of the lipid extracts were derivatized with N,N-dimethylglycine for analysis of DAG (6). Prepared samples were infused directly to TSQ Vantage triple quadrupole mass spectrometer (Thermo Fisher Scientific TSQ Vantage, San Jose, CA) equipped with an automated nanospray device (Triversa Nanomate, Advion Biosciences, Ithaca, NY). Multidimensional mass spectrometry- shotgun lipidomics (MDMS-SL) analysis of various lipid classes was performed according to published methods. Identification and quantification of PC, PE, PI, PS, LPC, LPE, Cer, CAR, SM, DAG, and TAG was performed using in- house automated software. Different modes and MS or MS/MS scans specific for each class of lipids are specified elsewhere (6-10). Quantification of each lipid species was carried out based on the internal standard addition. Total CL, PA, PG were identified and quantified based on the full MS scan acquired on Thermo Q Exactive Plus with heated ESI source mass spectrometer

(Thermo Fisher Scientific) equipped similarly with an automated nanospray device. To differentiate PG from Bis(Monoacylglycero)Phosphate (BMP) lipids we used parallel reaction monitoring scan (PRM) of selected upregulated PG species. The quantification of PG versus BMP was based on the ratio of reporter ions of acyl chain with glycerol phosphate (acyl chain+136=A) and another glycol (A+74=B) calculated using in-house automated software (10,11).

SUPPLEMENTARY FIGURE LEGENDS

Fig. S1. Sustained high fat diet-induced obesity and hepatic steatosis in wild-type mice. (A) Body weights, and hematoxylin and eosin stained liver sections from **(B)** 40 week-old chow-fed mice and **(C)** 40 week-old mice fed at 60% kcal fat diet for 35 weeks. n = 6/group. ****, $P < 0.0001$ by Student's *t* test. Scale bar = 100 μm.

Fig. S2. Representative primary NMR spectra from hepatic venous effluent from portal vein perfusions. (A) ^{1}H-NMR spectrum from effluent. Chemical shifts corresponding to α-anomeric proton of glucose carbon #1, the methyl signal for βOHB, respective alpha-CH_2 signals from propionate and octanoate (curved arrows), referenced in ppm to TSP. **(B)** ^{2}H-NMR spectrum from monoacetone glucose derivatized from ^{13}C/^{2}H-labeled glucose in effluent from 60 minute portal vein perfusions using oxygenated buffer containing 0.2 mM unlabeled sodium octanoate and 3% $^{2}H_2O$, in the presence of sodium [U-^{13}C]propionate (0.2 mM). Each chemical shift corresponds to ^{2}H isotopic enrichment at each atomic position in monoacetone glucose. **(C)** ^{13}C-NMR spectrum from monoacetone [^{13}C/^{2}H]glucose derivatized from ^{13}C/^{2}H-labeled glucose in effluent, with focus on carbon #2. The isotopomer patterns result from ^{13}C spin-spin scalar coupling when labeled spins are bonded to each other. See Supplementary Methods for details. **H** corresponds to ^{2}H-

substitution of protons covalently bound to the glucose carbon number that follows it. **Q** corresponds to the quartet of ^{13}C resonances attributable to coupling among ^{13}C-labeled glucose carbons #1-3; **D23** corresponds the doublet of ^{13}C resonances attributable to coupling between ^{13}C-labeled glucose carbons #2-3; **D12** corresponds the doublet of ^{13}C resonances attributable to coupling between ^{13}C-labeled glucose carbons #1-2; **S** corresponds to the signal comprised of ^{13}C-labeling of glucose carbon #2.

Fig. S3. Hepatic fluxes elevated in livers of sustained high fat diet-fed wild-type mice. (A) Glycogen, **(B)** glycerol, and **(C)** PEP flux to hepatic glucose production obtained by ^{2}H-NMR of monoacetone [$^{13}C/^{2}H$]glucose from effluent derived from 60 minute portal vein perfusions using oxygenated buffer containing 0.2 mM unlabeled sodium octanoate and 3% $^{2}H_2O$, in the presence of sodium [U-^{13}C]propionate (0.2 mM). **(D)** Relative contributions of glycogen, glycerol, and PEP to hepatic glucose production (derived from data presented in panels **(A-C)** and **Fig. 1A**). **(E)** Pyruvate cycling and **(F)** anaplerosis determined by ^{13}C-NMR from the same monoacetone [$^{13}C/^{2}H$]glucose obtained from these perfusions. Upper panels of **(C, E, F)** are absolute flux rates, and lower panels correspond to fluxes normalized to TCA cycle flux (whose data are presented in **Fig. 1D**). n = 6/group. ****, $P < 0.0001$; ***, $P < 0.001$; **, $P < 0.01$ by Student's *t* test.

Fig. S4. Unchanged abundances of phosphorylated and total glycogen synthase in livers of ketogenesis insufficient mice. Immunoblots for the phosphorylated (serine 641, inactivated) version of the liver/muscle isoforms of glycogen synthase (p-GS), total liver/muscle GS, and actin, acquired from protein lysates from livers of animals in the **(A)** random fed state or livers acquired or **(B)** at the end of a 60 minute metabolic perfusion using octanoate-containing oxygenated buffer.

Fig. S5. Ketogenesis insufficient mice exhibit markedly augmented glycogen-sourced hepatic glucose production that is not reversed by supplying exogenous ketone bodies. Sixty-minute portal vein perfusions were performed using oxygenated buffer containing 0.2 mM unlabeled sodium octanoate and 3% $^{2}H_2O$, 0.2 mM sodium [U-^{13}C]propionate, in the absence or presence of supplemented unlabeled ketone bodies in the indicated concentrations. **(A)** Glucose production (determined by ^{1}H-NMR; the first two bars on the left are presented for comparison and represent the same data as the middle two bars in **Fig. 2C**), **(B)** glycogenolysis flux (determined by ^{2}H-NMR of monoacetone [^{13}C/^{2}H]glucose; the first two bars on the left are presented for comparison and represent the same data as the middle two bars in **Fig. 2D**), **(C)** glycerol supported flux to glucogenogenesis (determined by ^{2}H-NMR of monoacetone [^{13}C/^{2}H]glucose; the first two bars on the left are presented for comparison and represent the same data as the middle two bars in **Fig. 2E**), **(D)** phosphoenolpyruvate (PEP) supported flux to glucogenogenesis (determined by ^{2}H-NMR of monoacetone [^{13}C/^{2}H]glucose; the first two bars on the left are presented for comparison and represent the same data as the middle two bars in **Fig. 2F**), **(E)** Relative contributions of glycogen, glycerol, and PEP to hepatic glucose [derived measurements from data presented in panels **(A-D)**]. n = 6-13/group. **, $P < 0.01$; *, $P < 0.05$ by two-way ANOVA with Tukey post-hoc test.

Fig. S6. Mass spectrometry-based untargeted metabolomics and shotgun lipidomics studies of ketogenesis insufficient livers. (A) XCMS Online cloud plot of 758 dysregulated chemical features in HMGCS2 ASO-treated livers compared with those of control livers. The radius (upregulated and downregulated features relative to controls are green and red, respectively) and shading darkness of each circle are proportional to each circle's fold-change and *P* value, respectively. **(B)** Radial plot of molar concentrations of the total pools of

phosphatidylethanolamines (PEs), phosphatidylinositol (PIs), lyso-phosphatidylcholines (LPCs), triacylglycerol (TAGs), and diacylglycerols (DAGs). Each segment radiating from the center represents an individual biological replicate. **(C)** Radial plot of molar concentrations of the total pools of ceramides (Cer), lyso-phosphatidylethanolamines (LPEs), sphingomyelins (SMs), and phosphatidylserines (PSs).

Fig. S7. Bis(monoacylglycero)phosphate accumulation in livers with relative or absolute ketogenic insufficiency. (A) Overview of phosphatidylglycerol (PG) metabolism. **(B)** mRNA abundances in liver for encoded mediators of PG metabolism. **(C)** Normalized protein abundances (by immunoblot) of α/β-hydrolase domain-containing 6 (ABDH6) in livers. **(D)** Total cholesterol (free + esterified) hepatic contents. Lipidomics (MS/MS) quantifications of **(E)** *m/z* 773, **(F)** *m/z* 819, and **(G)** *m/z* 865 PG and BMP species. **(F)** Serum total ketone body concentrations in *db/db* mice and controls. **C**, control ASO; **H**, HMGCS2 ASO. n = 5/group. *, $P < 0.05$ by two-way ANOVA with Bonferroni post-hoc test or Student's *t* test, as appropriate.

REFERENCES

1. Jin ES, Jones JG, Merritt M, Burgess SC, Malloy CR, Sherry AD. Glucose production, gluconeogenesis, and hepatic tricarboxylic acid cycle fluxes measured by nuclear magnetic resonance analysis of a single glucose derivative. *Analytical Biochemistry*. 2004;327(2):149-155.

2. Huang X, Chen YJ, Cho K, Nikolskiy I, Crawford PA, Patti GJ. X13CMS: global tracking of isotopic labels in untargeted metabolomics. *Anal Chem*. 2014;86(3):1632-1639.

3. Cotter DG, Ercal B, Huang X, et al. Ketogenesis prevents diet-induced fatty liver injury and hyperglycemia. *J Clin Invest*. 2014;124(12):5175-5190.

4. Mahieu NG, Genenbacher JL, Patti GJ. A roadmap for the XCMS family of software solutions in metabolomics. *Current Opinion in Chemical Biology*. 2016;30(Supplement C):87-93.

5. Mahieu NG, Spalding JL, Patti GJ. Warpgroup: increased precision of metabolomic data processing by consensus integration bound analysis. *Bioinformatics*. 2016;32(2):268-275.

6. Wang M, Hayakawa J, Yang K, Han X. Characterization and quantification of diacylglycerol species in biological extracts after one-step derivatization: a shotgun lipidomics approach. *Anal Chem*. 2014;86(4):2146-2155.

7. Yang K, Han X. Accurate quantification of lipid species by electrospray ionization mass spectrometry - Meet a key challenge in lipidomics. *Metabolites*. 2011;1(1):21-40.

8. Yang K, Cheng H, Gross RW, Han X. Automated lipid identification and quantification by multidimensional mass spectrometry-based shotgun lipidomics. *Anal Chem*. 2009;81(11):4356-4368.

9. Wang M, Fang H, Han X. Shotgun lipidomics analysis of 4-hydroxyalkenal species directly from lipid extracts after one-step in situ derivatization. *Anal Chem*. 2012;84(10):4580-4586.

10. Wang C, Wang M, Han X. Comprehensive and quantitative analysis of lysophospholipid molecular species present in obese mouse liver by shotgun lipidomics. *Anal Chem*. 2015;87(9):4879-4887.

11. Han X, Yang J, Cheng H, Ye H, Gross RW. Toward fingerprinting cellular lipidomes directly from biological samples by two-dimensional electrospray ionization mass spectrometry. *Anal Biochem*. 2004;330(2):317-331.

d'Avignon et al., Fig. S1

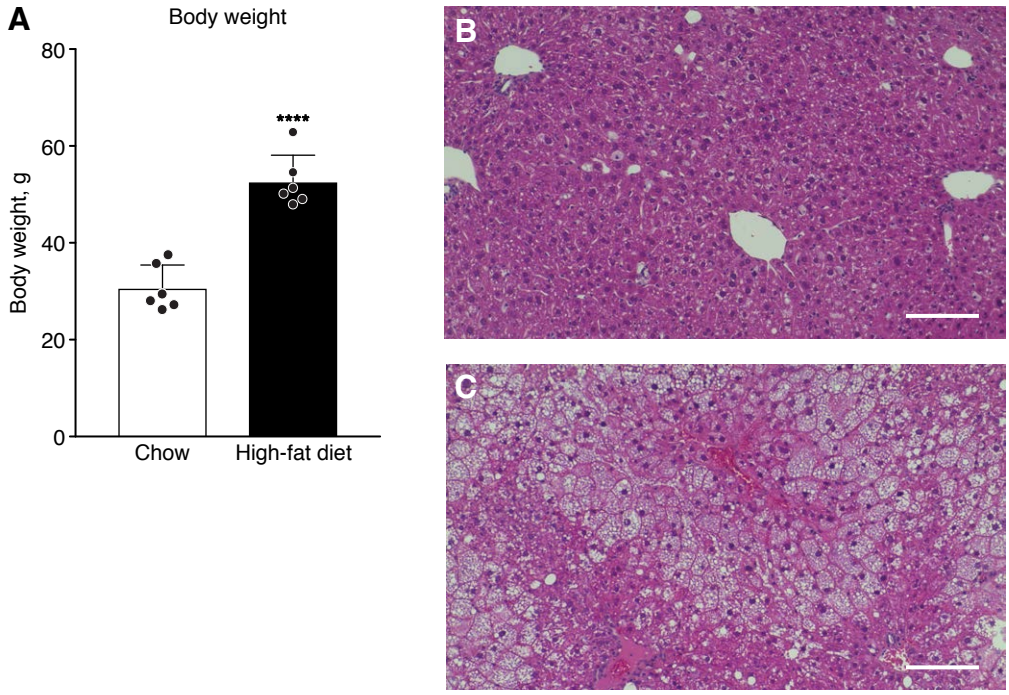

d'Avignon et al., Fig. S2

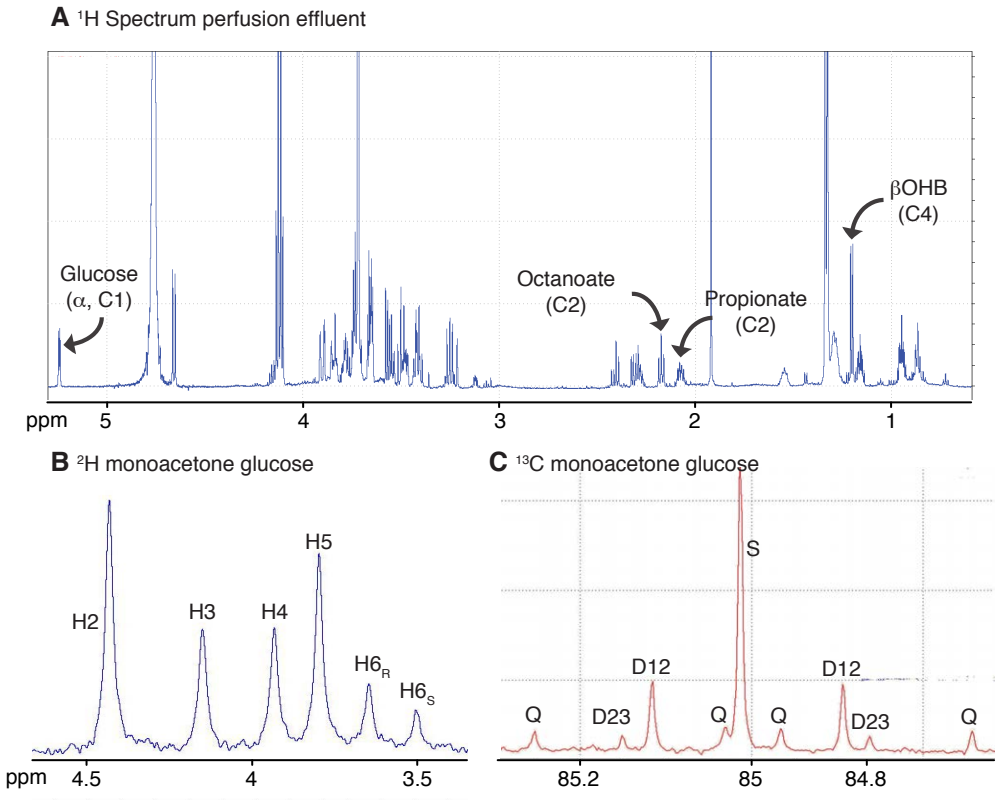

d'Avignon et al., Fig. S3

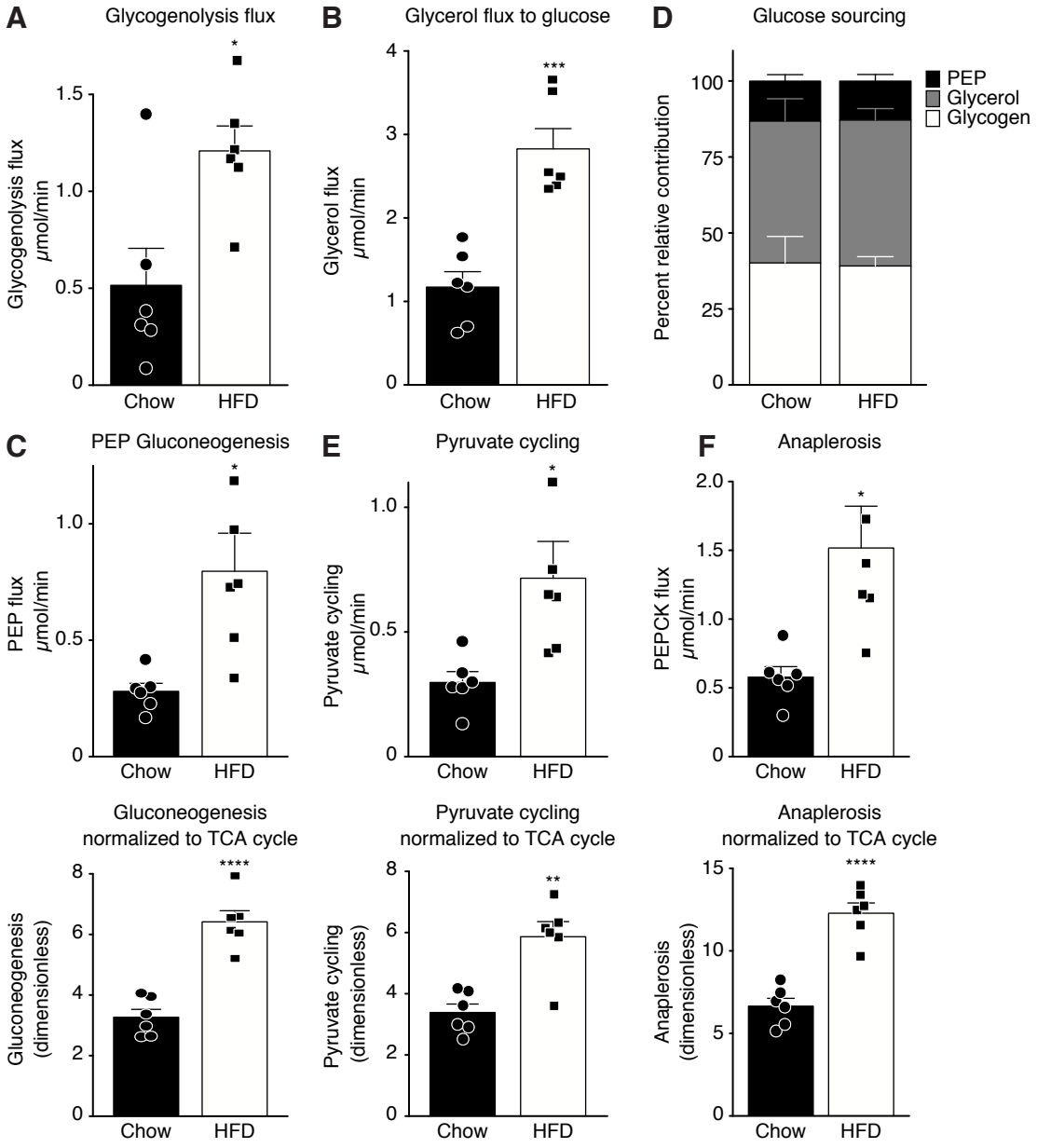

d'Avignon et al., Fig. S4

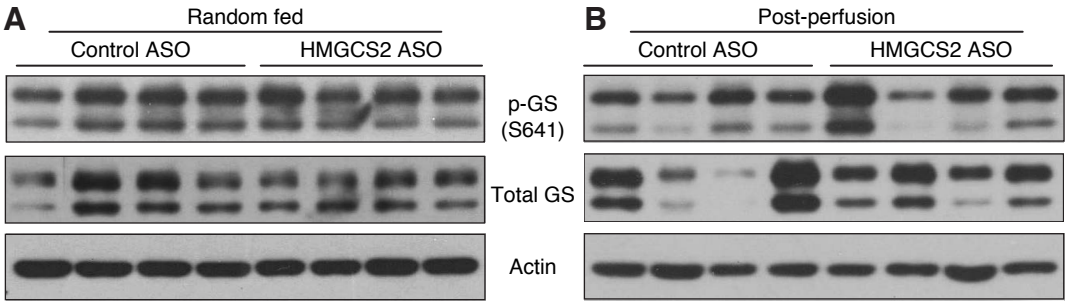

d'Avignon et al., Fig. S5

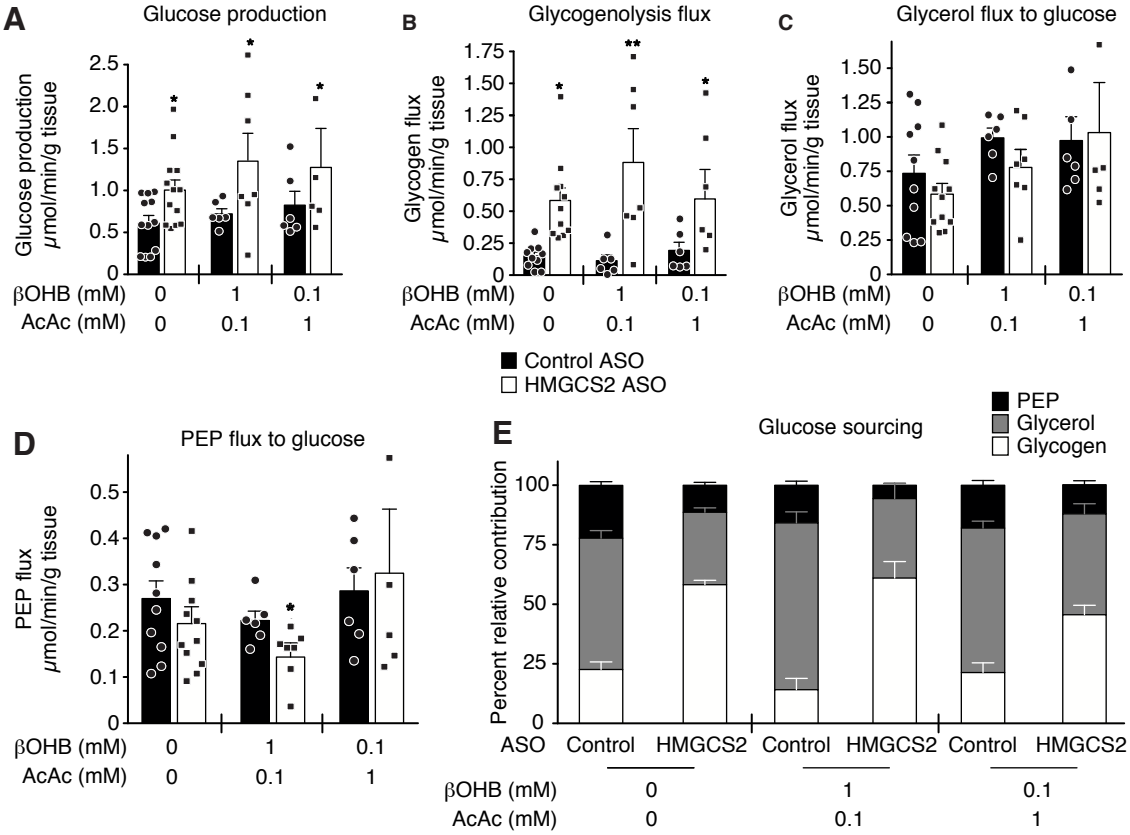

d'Avignon et al., Fig. S6

A

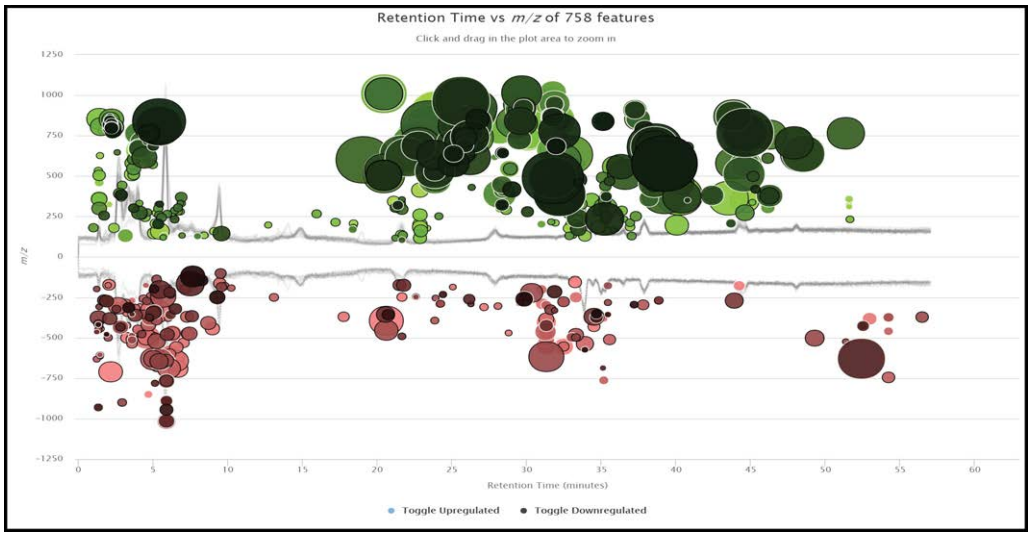

B

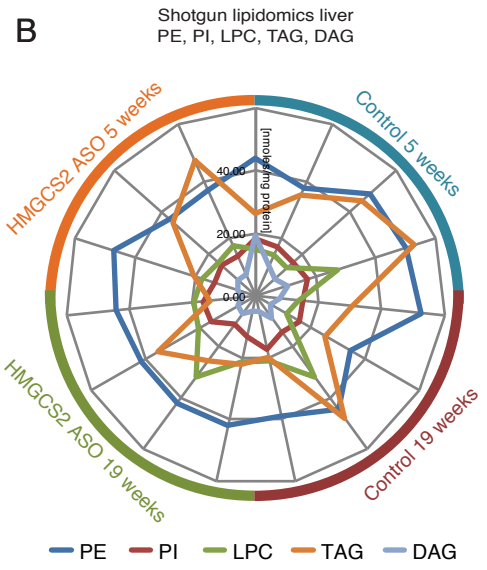

C

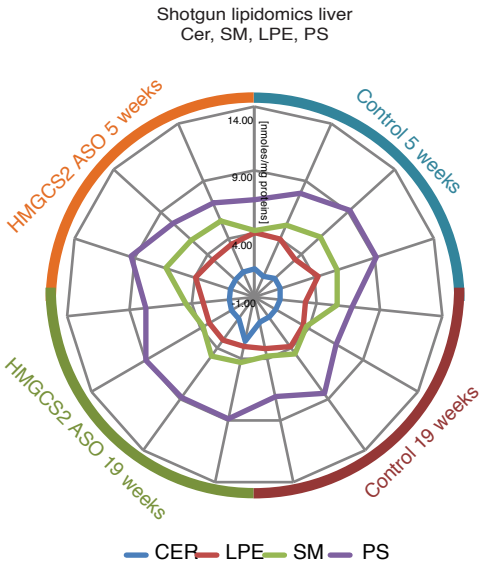

d'Avignon et al., Fig. S7